RSC Advances

This is an *Accepted Manuscript*, which has been through the Royal Society of Chemistry peer review process and has been accepted for publication.

Accepted Manuscripts are published online shortly after acceptance, before technical editing, formatting and proof reading. Using this free service, authors can make their results available to the community, in citable form, before we publish the edited article. This *Accepted Manuscript* will be replaced by the edited, formatted and paginated article as soon as this is available.

You can find more information about *Accepted Manuscripts* in the Information for Authors.

Please note that technical editing may introduce minor changes to the text and/or graphics, which may alter content. The journal's standard Terms & Conditions and the Ethical guidelines still apply. In no event shall the Royal Society of Chemistry be held responsible for any errors or omissions in this *Accepted Manuscript* or any consequences arising from the use of any information it contains.

ROYAL SOCIETY OF CHEMISTRY

www.rsc.org/advances

Please do not adjust margins

Journal Name

ARTICLE

Fabrication and Ionic Transportation Characterization of Funnel-Shaped Nanochannels

Received 00th January 20xx,
Accepted 00th January 20xx

DOI: 10.1039/x0xx00000x

www.rsc.org/

Kai Xiao,[a] Pei Li,[b] Ganhua Xie,[a] Zhen Zhang,[a] Liping Wen*[c] and Lei Jiang*[b,c]

Solid-state nanochannel is an emerging field of interest because of its exhibition similar properties but more stable to the biological nanopores. However, all the existing solid-state nanochannels, such as conical-shaped nanochannel, rely on a limited critical region at the tip side and thus demonstrate poor controllability of the orientation and magnitude of the ionic rectification. In this work, we demonstrate the fabrication of funnel-shaped nanochannels with a gradual structural transformation. The longer crucial regions can be well controlled by tuning the etching temperature. In addition, the rectification ratio can increase from about 3 to 6 by introducing the longer crucial region. With the finite-element computations based on the Poisson–Nernst–Planck (PNP) equations, it can be found that the increased longer crucial region could contribute to the asymmetric ion transportation. The funnel-shaped nanochannels with enhanced asymmetric ion transportation may find applications in the fields of materials, electronics, and life sciences.

Introduction

Biological nanochannels play key roles in basic biochemical processes in living systems,[1] which can be realized mainly by three characteristic features including ionic selectivity, ionic rectification and ionic gating. Inspired by the protein channels, various solid-state nanopores and nanochannels have been created and functionalized to realize these functions to simulate the process of ionic transport in living organisms.[2-7] Antecedent works have shown that ion current rectification and permselectivity in confined channels are a consequence of electrostatic interactions between the substrate of the channel and the electrolyte solution.[8] Under asymmetric conditions (i.e., an asymmetric-shaped channel or a symmetric channel with asymmetric surface charges), the internal potential has been shown to be asymmetric. Thus, the ions with the opposite charge to the substrate would accumulate near the channel surface, but the distribution would be non-uniform along the axis due to the asymmetric channel structure. Considering the matching between Debye length and the diameter of the channel, this non-uniformity is a prerequisite for traditional fluidic diodes that are based on asymmetric nanochannels. But under symmetric conditions (i.e., a cylindrical channel), a Debye length on the order of the nanochannel does not result in ion current rectification due to the lack of broken symmetry in their electrochemical potential. Therefore, asymmetric factors (i.e., asymmetric shape, surface charges and wettability) of the nanochannels are the foundation of the rectification and permselectivity. Until now, different approaches and materials have been proposed to construct and functionalize solid-state nanopores and nanochannels to meet the requirements of ion current rectification and permselectivity, which are the basic of sensing, energy transition, and filtrating.[9-13]

Early works in this field started with the α-hemolysin protein nanochannel which consists of a single protein nanochannel embedded within a lipid bilayer membrane.[14-16] Typically, the protein-based nanochannels and their embedding lipid bilayers can become unstable if external parameters such as pH, salt concentration, temperature and mechanical stress are changed. Hence the focus has been moving towards solid-state nanochannels due to their high stability, durability, shape-controllability and tailorable surface properties. The most widely used materials for nanochannels are polymers including polycarbonate (PC),[17, 18] polyethylene terephthalate (PET),[19-21] polyimide (PI),[22-24] silicon nitride[25-27], silicon,[28, 29] and glass.[30, 31] By now, a variety of approaches have been used to prepare abiotic nanochannels for resistive-pulse sensing including track-etching,[32, 33] focused ion beam sculpting,[27, 34] electron-beam lithography,[34] soft lithography[35, 36] and film embedding of carbon nanotubes.[37] Among them the track-etched method for the polymer solid-state nanochannel proves to be a surprisingly versatile tool for contemporary biotechnology and has been used to fabricate solid-state nanochannels both symmetric and asymmetric. Different shapes of nanochannels, such as cylindrical shape,[38, 39] hour-glass shape,[40, 41] cigar-like shape,[42-44] bullet-like shape,[45, 46] conical shape,[22, 47-49] funnel-shaped,[50-52] and dumbbell-shaped nanochannels have been prepared by controlling a different potential and by adding surfactants or organic solvents to the

[a] Beijing National Laboratory for Molecular Sciences (BNLMS), Key Laboratory of Green Printing, Institute of Chemistry, Chinese Academy of Sciences, Beijing 100190 (P.R. China)
[b] Key Laboratory of Bio-Inspired Smart Interfacial Science and Technology of Ministry of Education, School of Chemistry and Environment, Beihang University, Beijing 100191, P. R. China
[c] Laboratory of Bioinspired Smart Interfacial Science, Technical Institute of Physics and Chemistry, Chinese Academy of Sciences, Beijing 100190 (P.R. China)
Electronic Supplementary Information (ESI) available: [details of any supplementary information available should be included here]. See DOI: 10.1039/x0xx00000x

RSC Advances Accepted Manuscript

Please do not adjust margins

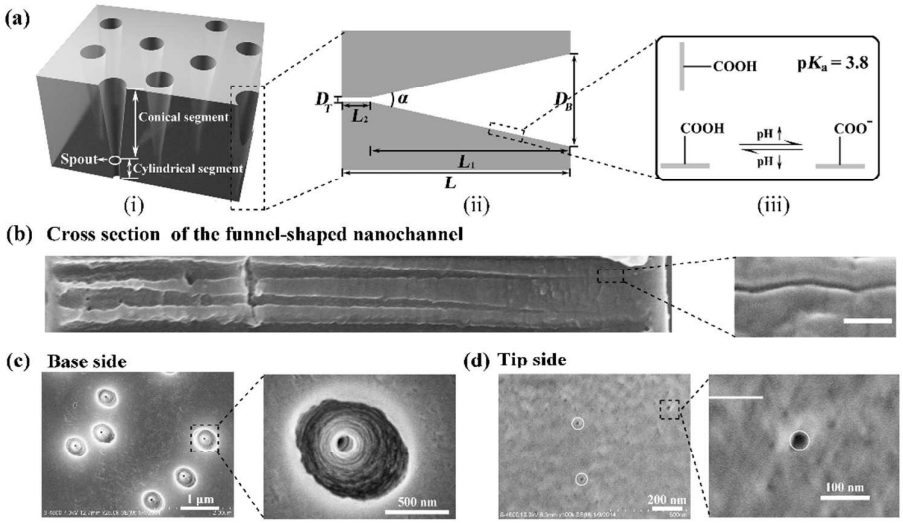

Fig. 1 (a) Scheme of funnel-shaped nanochannels in PET film and the inner surface properties. (b) SEM images of the cross section of the funnel-shaped nanochannel and partial enlarged drawing cylindrical segment. (c) SEM image of the base side of the funnel-shaped nanochannels and partial enlarged drawing. (d) SEM images of the tip side of the funnel-shaped nanochannels and partial enlarged drawing.

etchant solution during etching process. However, the existing nanochannels, such as conical-shaped nanochannel, rely on a limited critical region at the tip side and thus demonstrate poor controllability of the orientation and magnitude of the ionic rectification.[51, 53-55] Therefore, it is necessary to fabricate a novel solid-state nanochannel system with a longer crucial region to realize complicated functions by precise controlling its asymmetric shape.

Here, the fabricated funnel-shaped nanochannels comprised three parts, a conical segment, a spout and a cylindrical segment (Fig. 1a). By controlling the etching temperature, the position of the spout can be tuned precisely. In practical terms, the length of the conical segment was validated to be longer than 10 μm, an overwhelming majority of the 12 μm thickness of the PET film while the cylindrical segment was confined to shorter than 2 μm. Meanwhile, the large opening side diameters and cone angles on the conical segment increased with the etching temperature. These funnel-shaped nanochannels exhibited superior asymmetric ion transportation properties compared with conical nanochannels, which can be further proved by the finite-element computations based on the Poisson–Nernst–Planck (PNP) equations.

Experiments

Polyethylene terephthalate (PET) membrane preparation

Polymer foils of Polyethylene terephthalate (PET) (Hostaphan RN 12, Hoechst, density of $2*10^7/cm^2$) of 12 μm thickness were irradiated at the linear accelerator UNILAC (GSI, Darmstadt) with swift heavy ions (Au) having an energy of 11.4 MeV per nucleon. The fabrication of nanochannels in a PET membrane was accomplished by asymmetric etching of the damage trail of heavy ions which passed through this membrane. Before the chemical etching process, the polymer films were exposed to the UV light (365 nm, 20 W), for 1h from each side.

Fabrication of the Funnel-Shaped Nanochannels

The fabrication and Current-Voltage (*I-V*) recordings device was shown in Fig. S1. In the fabrication process, the device was heat to control the etching temperature. The following were the etching and stopping solutions for the etching of PET: 9 M NaOH for etching, 1 M KCl + 1 M HCOOH for stopping. The etching process was carried at varied temperature (25 °C，30 °C，40 °C，50 °C，60 °C). Firstly, the track-etched membrane was mounted between two halves of a conductivity cell and Pt electrodes were used to apply a transmembrane potential.; Secondly, one of the cell was filled with etching solution while another was filled with stopping solutions. During etching, a potential of 1 V was applied across the membrane in order to monitor the breakthrough of the nanochannel and observe the current flowing through the nascent nanochannels. The current remains zero as long as the channel is not yet etched through, and after the break through the increase of current is observed. The etching process was stopped when the current reached a certain value. Then the membrane was soaked in MilliQ water (18.2 MΩ) to remove residual salts.

Current Measurement

The ionic transport properties of the nanochannels were studied by measuring ionic current through the multinanochannels. Ionic current was measured by a Keithley 6487 picoammeter (Keithley Instruments, Cleveland, OH). The funnel-shaped nanochannels membrane was mounted between two chambers of the etching cell mentioned above. The *I-V* curves were adjusted to zero current at zero voltage to remove small offsets experienced between runs. All measurements were carried out at room temperature and *I-V* behaviour was examined with 0.1 M KCl neutral aqueous solution. In all experiments, Ag/AgCl electrodes were used to apply a transmembrane potential across the film, and the positive electrode was at the base of the funnel-shaped nanochannels and the negative electrode at the tip of the funnel-shaped nanochannel. The main transmembrane potential used in this work was stepped at 0.2 V/step for 1 s/step (0.2 V/s) from -2 to +2 V, with its period of 40 s.

Results and discussion

Morphology of the funnel-shaped nanochannels

The dimension and the morphology of the funnel-shaped nanochannels were characterized by the scanning electron microscope (SEM). Fig. 1b-d showed the SEM images of the fracture and the surface of the funnel-shaped nanochannels etched at 40 °C. Fig. 1b demonstrated the cross section of funnel-shaped

RSC Advances Accepted Manuscript

 This journal is © The Royal Society of Chemistry 20xx

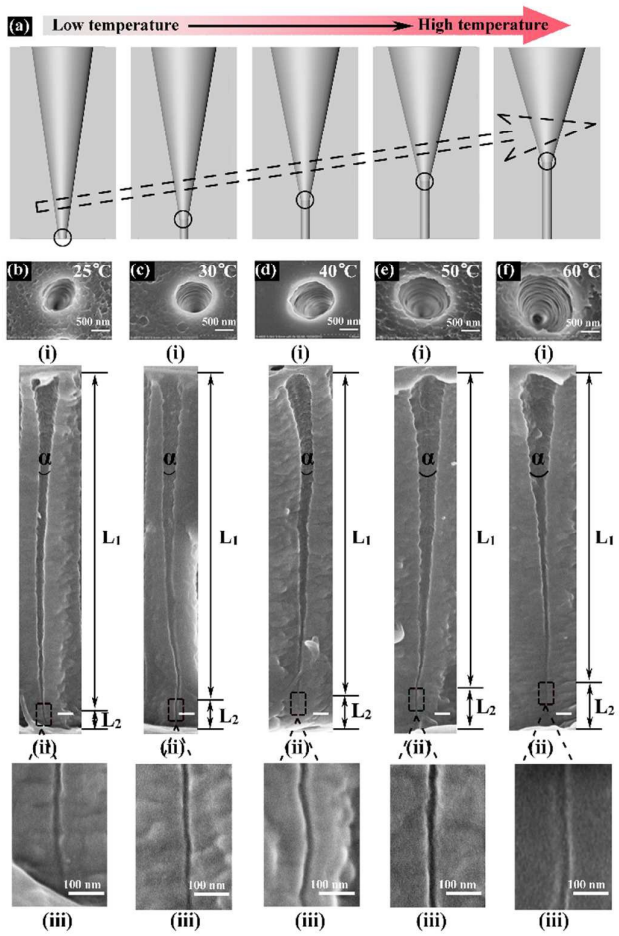

Fig. 2 (a) Schematic diagram of asymmetric nanochannels from the conical-shaped to the funnel-shaped by changing the etching temperature. (b-f) SEM images of the funnel-shaped nanochannel with varied temperature (left to right: 25 °C，30 °C，40 °C，50 °C，60 °C respectively). i: Top view. ii: Cross section (scale bar 100 nm). iii: Enlarged cylindrical segments.

nanochannel and partial enlarged drawing of the cylindrical segment. It can be clearly found that the asymmetric nanochannel consists of the conical segment and the cylindrical segment. The base side of the conical segment is about 1000 nm while the diameter of the cylindrical segment is about 15 nm. Fig. 1c illustrated the top view of the base side of the funnel-shaped nanochannels and the enlarged drawing, which proved the taper change in conical segment. Fig. 1d showed the top view of the tip side of the nanochannels and partial enlarged drawing. The tip diameter is about 15 nm, which is equal to the diameter of the cylindrical segment. These results complement the results related to the cross sections of the funnel-shaped nanochannel and verify the transformation from a conical structure to a cylindrical segment indirectly.

Funnel-shaped nanochannels with varied etching temperatures

Five funnel-shaped nanochanels with different geometry were prepared under etching temperature of 25 °C, 30 °C, 40 °C, 50 °C, and 60 °C, respectively. By adjusting the etching temperature, the base side diameter, the cone angle and the spout position of the funnel-shaped nanochannels can be precisely controlled (Fig. 2a). Fig. 2b-f demonstrated the SEM images of the top views and cross sections of these funnel-shaped nanochannels. The difference in base diameters (Fig. 2b i-f i) and cone angles (Fig. 2b ii-f ii) of the nanochannel prepared under different etching temperature could be observed clearly. The diameters of the base sides increased from ~800 nm to ~1400 nm (Fig. 3a) while the cone angles increased from ~3.9° to ~7.8° (Fig. 3b) with the etching temperature rising from 25 °C to 60 °C. Table S1 showed the statistical diameters and cone angles, which were analyzed based on SEM images. Meanwhile, the tip diameters could be calculated by Equation 1.[56]

$$D_T = \left[\frac{4g(1-V_B/V_T)}{D_B^{\,2}} - \left(\frac{k\pi}{V_T}\right)g\left(\frac{U}{I}\right)\right]^{-1/2} \quad (1)$$

Where V_B and V_T are the bulk etching speed and rack etching speed, D_T and D_B are the tip and base diameters, k is the specific conductivity of the electrolyte, U and I are the applied voltage and measured ionic current in the pore conductivity measurement, respectively. The calculated tip diameters also increased along with the etching temperature from ~12 nm to ~20 nm, which showed consistency with the SEM images (Fig. 2b iii-f iii).

Meanwhile, the length of the cylindrical segment, which can be represented by the distance between spout and the tip of the nanochannel, also can be obtained from the SEM images. Under 25 °C, the cylindrical segment of the funnel-shaped nanochannel was about 220 nm, which can be neglected compared with the entire channel. It is to say, this nanochannel is an approximate cone. The cylindrical segment length increased along with the etching temperature and reached to 515 nm, 1000 nm, 1114 nm and 1979 nm for the 30 °C, 40 °C, 50 °C and 60 °C, respectively (Fig. 3c red line). In order to further prove the relationship between the spout position and etching temperature, we suggested a theoretical model for these funnel-shaped asymmetric nanochannels. The following formula was used to calculate the location of the transition point:

$$L_2 = L - L_1 = L - \frac{(\frac{D_B}{2} - \frac{D_T}{2})}{\tan\frac{\alpha}{2}} \quad (2)$$

Where L is the entire length of the channel, L_1 is the length of the cone, L_2 is the distance between the tip side and the transition point, α is the angle of the conical segment, D_B and D_T are the base and tip diameters of the conical segment. Then a quantitative relationship between the length of the cylindrical segment L_2 and the parameters D_B, D_T, α from the conical segment can be established by Equation 2. Theoretical proof shows that the spout is close to the tip side (about 220 nm from tip side) at relatively low temperature (25 °C). When the temperature rose to 60 °C, the length of the cylindrical segment could be increased to about 1900 nm. And the length of the cylindrical segment increased almost linearly along with the increasing etching temperature (Fig. 3c, black line), which could be reproduced by the experimental curves obtained from SEM images.

RSC Advances Accepted Manuscript

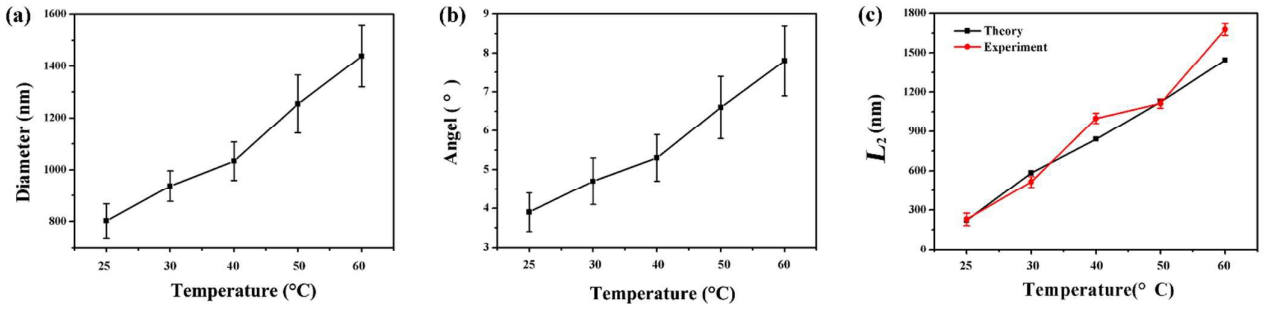

Fig. 3 (a) The base diameter of the conical segment of the funnel-shaped nanochannel distribution with temperature. (b) Conical angle of the conical segment of the funnel-shaped nanochannel distribution with temperature. (c) The location of the spout observed from SEM images (experiment: red line) and calculated by the model (theory: dark line).

The relationship between the track etching velocity and the etching temperature, which can be characterized by measuring the break-through ionic current in the track-etching process, has also been studied. Fig. 4 shows the changes of track etching velocity with the etching temperature that ranged from 25 °C to 60 °C in three parallel experiments. The etching velocities were 0.21 μm/min, 0.58 μm/min, 0.82 μm/min, 1.21μm/min, and 2.3 μm/min

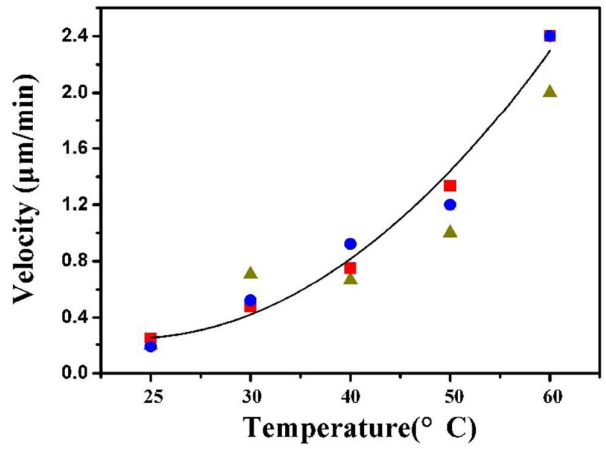

Fig. 4 Relationship between the etching velocity and the temperature (25 °C，30 °C，40 °C，50 °C，60 °C). Red quadrate ■, blue circle ● and dark yellow triangle ▲ represent three parallel experiments. Black line is the polynomial simulation curve.

under 25 °C, 30 °C, 40 °C, 50 °C, and 60 °C, respectively, which accorded with binomial simulation (Fig. 4 black line). This nonlinear rising tendency manifests indirectly that cylindrical segment will be longer if the etching temperature is higher.

Etching mechanism

The etching mechanism is schematically shown in Fig. 5a and 5b. At low temperature (25 °C), the V_{LT} (low temperature track etching velocity) on the direction along the damage trail is faster than the V_{LB} (low temperature buck etching velocity) on the direction perpendicular to the damage trail of heavy ions which passed through the membrane. After a short time of breakthrough, the etching process was stopped before the alkali diffuses to the region beyond the damage trail. Hence, a smallish cylindrical segment was formed at the tip side of the nanochannel (Fig. 5a). While at high temperature (60 °C), the V_{HT} (high temperature track etching velocity) is incomparable fast compared with the V_{LT} and V_{HB} (high temperature bulk etching velocity) and the etching process was stopped as soon as breakthrough, which means that the tip side has not enough time to be etched, and thus a cylindrical segment would be obtained (Fig. 5b). In fact, the etching rate ratio (V_{LT}/ V_{LB}) can reach to 1000 under low temperature (25 °C) while high temperature would further expand the etch rate ratio (V_{HT}/ V_{HB}). Hence, the funnel-shaped nanochannel with different cylindrical segments can be generated by changing the etching temperature.

Ion Transport Properties

Ionic transport properties of these funnel-shaped nanochannels have been examined by current measurements. The transmembrane ionic current was recorded under symmetrical electrical conditions using 0.1 M KCl (pH≈7) solution in both halves of the conductivity cell. Fig. 6a shows *I-V* properties of the funnel-shaped nanochannels that were prepared under different etching temperatures from 25 °C to 60 °C, from which it can be found that the *I-V* curves associated with ionic migration through these nanochannels are nonlinear. These funnel-shaped nanochannels with ion-current rectification property have been observed previously in a variety of asymmetrical nanochannels and nanotubes, and experiments prove that ion-current rectification is inherent to asymmetry, *e.g.,* conical nanochannel systems with excess surface charge.[57, 58] And the extent to which the funnel-shaped nanochannel rectifies the ion current flowing through it can be quantified by the rectification ratio, defined as the absolute value of the current obtained at -2 V divided by the current obtained at +2 V. Clearly, the rectification ratios increased gradually from about 3 to 6 along with the etching temperature (Fig. 6b blue line). To the conical nanochannel, only weak ion-rectifying property was obtained because the transport properties were determined by the physical and chemical properties of the nanoscale critical point (tip side) of the channel. Nevertheless, with an increased critical region, the cylindrical segment has tremendous potential for ion selectively and can enhance the rectification ratio.

Meanwhile, the ion current at constant voltage (-2 V) decreased significantly from 3.2 μA to 1.5 μA (Fig. 6b dark line). It also can be explained by the length of the cylindrical segment, which is comparable to the Debye length.[50, 51] In the nanochannel, the charged nanosized crucial region (the tip side of the conical and the cylindrical segment of the funnel-shaped nanchannel) can adsorb

RSC Advances Accepted Manuscript

This journal is © The Royal Society of Chemistry 20xx

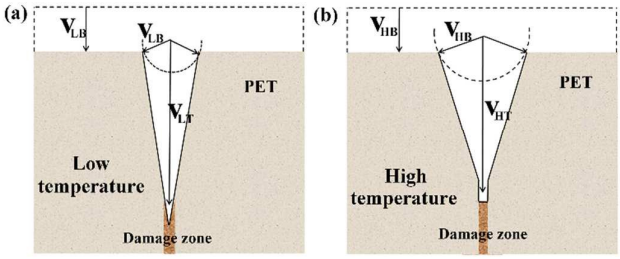

Fig. 5 (a) Schematic of etched ion tracks in low temperature environment. (b) Schematic of etched ion tracks in high temperature environment.

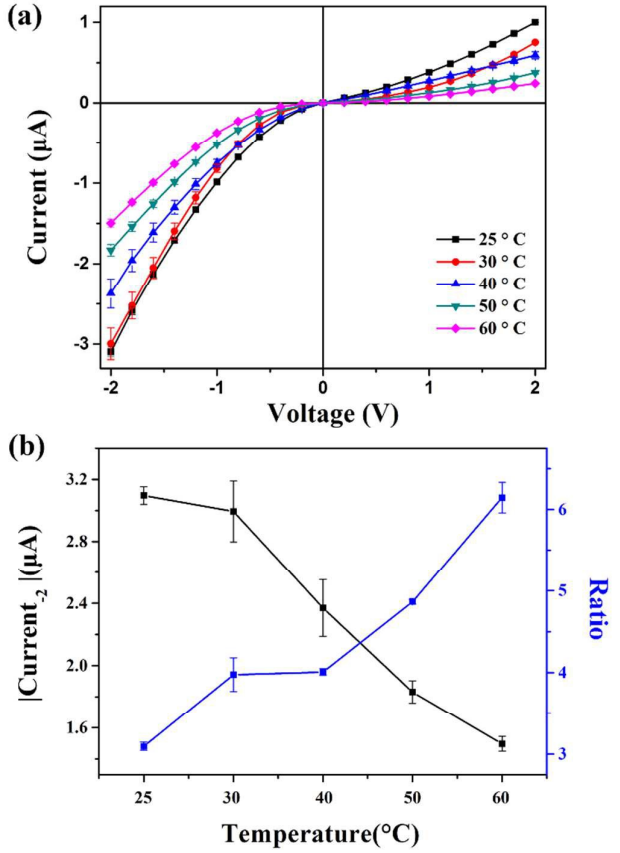

Fig. 6 (a) Current-voltage curves for funnel-shaped nanochannels with varied temperature. (b) Ion current at constant voltage (-2V) and rectification ratio of the funnel-shaped nanochannels with varied temperature.

the counter-ions in the electrolyte, then block the ion transportation. The resistance of the ions is proportional to the length of the cylindrical segment because of the interaction force with charged channel wall. As a result, the funnel-shaped nanochannel with longer crucial region has a smaller ionic current.

Theoretical calculation based on Poisson-Nernst-Planck (PNP)

Antecedent works have shown that ion current rectification could be observed in nanochannels with three conditions: the accordance between the diameter of the channel and the length of the electrical double layer, the excess surface charge and the

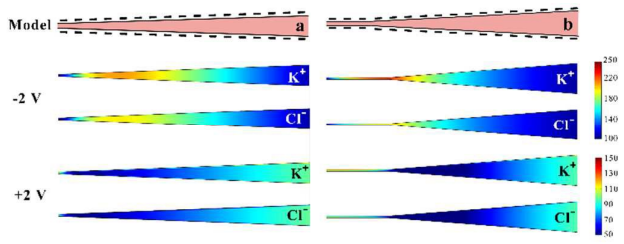

Fig. 7 (a) Concentration profile (K^+ and Cl^-) of numerical simulation by 2D configuration of the conical-shaped nanochannel under -2 V and +2 V. (b) Concentration profile (K^+ and Cl^-) of numerical simulation by 2D configuration of the funnel-shaped nanochannel under -2 V and +2 V.

interactions of ions with the pore wall.[59-61] To get a further understanding of the ions

transportation in the funnel-shaped nanochannel, the model based on the Poisson–Nernst–Planck (PNP) equations is used to quantitatively describe the ion current in the nanochannel.[57, 62, 63] And finite-element computations were performed to solve simultaneously PNP equations for the ion concentration to better understand the shape-dependent *I-V* behaviours (Fig. S2). The ions concentration distribution (K^+ and Cl^-) can visually reflect the rectification ratio because the rectification effect stems from the accumulation and depletion of ions in the channel in response to different bias polarities. As shown in Fig. 7a, it can be clearly found that both the K^+ and Cl^- concentrations under -2 V are higher than that under +2 V to the conical-shaped nanochannels because the ions

would accumulate under negative voltage, resulting in high ion conduction. On the contrary, reversing the direction of the applied electric field move the ions in the outward direction from the channel, causing formation of a depletion zone and, consequently, a very low conductance of the nanochannel, which generate the rectification of ion current. The concentration distributions of the funnel-shaped nanochannel is similar with the conical-shaped nanochannel but more ions would accumulate in the spout and longer cylindrical segment, which is comparable to the Debye length, (Fig. 7b) and thus lead to a higher rectification ratio. In addition, the negative charged nanosized crucial region (the tip side of the conical and the cylindrical segment of the funnel-shaped nanchannel) can adsorb the counter-ions (K^+) in the electrolyte, hence, the K^+ concentrations are higher than the Cl^- concentrations both in the conical and funnel-shaped nanochannel. Therefore, the ion concentration distributions simulated by finite-element simulations can provide direct and strong evidence for our experiment, which also have important ramifications for the application of such funnel-shaped nanochannels to biosensor designs.

Conclusions

In summary, we have shown that the funnel-shaped nanochannels with a gradual structural transformation can be fabricated by changing the track-etching temperature. The funnel-shaped nanochannels consist of three parts, the conical segment,

RSC Advances Accepted Manuscript

the cylindrical segment and the spout that connects the conical segment and the cylindrical segment. The spout position can be controlled by adjusting the etching temperature. Most importantly, the rectification ratio can increase from about 3 to 6 by introducing the longer crucial region. Meanwhile, the finite-element computations can match with the experimental results well. Such funnel-shaped nanochannels may find applications in the fields of materials, electronics, and life sciences.

Acknowledgements

This work was supported by the National Research Fund for Fu ndamental Key Projects (2013CB933000), the National Natural Science Foundation (21434003, 91427303, 21421061), and the Key Research Program of the Chinese Academy of Sciences (KJ ZD-EW-M03).The author thank the Material Science Group of GSI for providing the ion-irradiated samples.

Notes and references

1. B. Hille, *Ion channels of excitable membranes*, Sinauer Sunderland, MA, 2001.
2. K. Xiao, X.-Y. Kong, Z. Zhang, G. Xie, L. Wen and L. Jiang, *J. Photochem. Photobiol. C: Photochem. Rev.*, 2016, **26**, 31-47.
3. L. Wen, Y. Tian and L. Jiang, *Angew. Chem. Int. Edit.*, 2015, **54**, 3387-3399.
4. S. J. Kim, Y.-A. Song and J. Han, *Chem. Soc. Rev.*, 2010, **39**, 912-922.
5. H. Daiguji, *Chem. Soc. Rev.*, 2010, **39**, 901-911.
6. R. E. Gyurcsányi, *TrAC-Trend. Anal. Chem.*, 2008, **27**, 627-639.
7. C. R. Martin and Z. S. Siwy, *Science*, 2007, **317**, 331-332.
8. I. Vlassiouk and Z. S. Siwy, *Nano Lett.*, 2007, **7**, 552-556.
9. J.-Y. Lin, C.-Y. Lin, J.-P. Hsu and S. Tseng, *Anal. Chem.*, 2016, **88**, 1176-1187.
10. Z. Zhang, X.-Y. Kong, K. Xiao, Q. Liu, G. Xie, P. Li, J. Ma, Y. Tian, L. Wen and L. Jiang, *J. Am. Chem. Soc.*, 2015, **137**, 14765-14772.
11. L. Wen, K. Xiao, A. V. Sainath, M. Komura, X. Y. Kong, G. Xie, Z. Zhang, Y. Tian, T. Iyoda and L. Jiang, *Adv. Mater.*, 2016, **28**, 757-763.
12. M. Fujiwara and T. Imura, *ACS Nano*, 2015. **6**, 5705-5712.
13. J. D. Feng, K. Liu, R. D. Bulushev, S. Khlybov, D. Dumcenco, A. Kis and A. Radenovic, *Nat. Nanotechnol.*, 2015, **10**, 1070-1076.
14. T. Li, L. Liu, Y. R. Li, J. N. Xie and H. C. Wu, *Angew. Chem. Int. Edit.*, 2015, **54**, 7568-7571.
15.J. J. Kasianowicz, E. Brandin, D. Branton and D. W. Deamer, *Proc. Natl. Acad. Sci. U S A*, 1996, **93**, 13770-13773.
16. J. E. Gouaux, O. Braha, M. R. Hobaugh, L. Song, S. Cheley, C. Shustak and H. Bayley, *Proc. Natl. Acad. Sci. U S A*, 1994, **91**, 12828-12831.
17. C. C. Harrell, Y. Choi, L. P. Horne, L. A. Baker, Z. S. Siwy and C. R. Martin, *Langmuir.*, 2006, **22**, 10837-10843.
18. C. Schönenberger, B. Van der Zande, L. Fokkink, M. Henny, C. Schmid, M. Krüger, A. Bachtold, R. Huber, H. Birk and U. Staufer, *J. Phys. Chem. B*, 1997, **101**, 5497-5505.
19. P. Y. Apel, I. V. Blonskaya, O. L. Orelovitch, P. Ramirez and B. A. Sartowska, *Nanotechnology*, 2011, **22**, 175302.
20. K. Xiao, G. Xie, P. Li, Q. Liu, G. Hou, Z. Zhang, J. Ma, Y. Tian, L. Wen and L. Jiang, *Adv. Mater.*, 2014, **26**, 6560-6565.
21. M. Ali, S. Nasir and W. Ensinger, *Chem. Commun.*, 2015, **51**, 3454-3457.
22.L. P. Wen, Q. Liu, J. Ma, Y. Tian, C. H. Li, Z. S. Bo and L. Jiang, *Adv. Mater.*, 2012, **24**, 6193-6198.
23. A. Mara, Z. Siwy, C. Trautmann, J. Wan and F. Kamme, *Nano Lett.*, 2004, **4**, 497-501.
24.Z. Siwy, D. Dobrev, R. Neumann, C. Trautmann and K. Voss, *Appl. Phys. A*, 2003, **76**, 781-785.
25. D. J. Niedzwiecki, R. Iyer, P. N. Borer and L. Movileanu, *ACS Nano*, 2013, **7**, 3341-3350.
26. A. Han, M. Creus, G. Schürmann, V. Linder, T. R. Ward, N. F. de Rooij and U. Staufer, *Anal. Chem.*, 2008, **80**, 4651-4658.
27. J. Li, D. Stein, C. McMullan, D. Branton, M. J. Aziz and J. A. Golovchenko, *Nature*, 2001, **412**, 166-169.
28. R. Kox, C. Chen, G. Maes, L. Lagae and G. Borghs, *Nanotechnology*, 2009, **20**, 115302.
29. S. R. Park, H. Peng and X. S. Ling, *Small*, 2007, **3**, 116-119.
30. N. Laohakunakorn, V. V. Thacker, M. Muthukumar and U. F. Keyser, *Nano Lett.*, 2015, **15**, 695-702.
31. G. Wang, A. K. Bohaty, I. Zharov and H. S. White, *J. Am. Chem. Soc.*, 2006, **128**, 13553-13558.
32. P. Y. Apel, I. V. Blonskaya, S. N. Dmitriev, O. L. Orelovitch, A. Presz and B. A. Sartowska, *Nanotechnology*, 2007, **18**, 305302.
33. P. Apel, *Radiat. Meas.*, 2001, **34**, 559-566.
34. A. Storm, J. Chen, X. Ling, H. Zandbergen and C. Dekker, *Nat. Mater.*, 2003, **2**, 537-540.
35. O. A. Saleh and L. L. Sohn, *Nano Lett.*, 2003, **3**, 37-38.
36. J. Han and H. Craighead, *Science*, 2000, **288**, 1026-1029.
37. L. Liu, C. Yang, K. Zhao, J. Li and H.-C. Wu, *Nat. Commun.*, 2013, **4**.
38. N. Liu, Y. Jiang, Y. Zhou, F. Xia, W. Guo and L. Jiang, *Angew. Chem. Int. Ed.*, 2013, **52**, 2007-2011.
39. Q. H. Nguyen, M. Ali, V. Bayer, R. Neumann and W. Ensinger, *Nanotechnology*, 2010, **21**, 365701.
40. X. Hou, F. Yang, L. Li, Y. L. Song, L. Jiang and D. B. Zhu, *J. Am. Chem. Soc.*, 2010, **132**, 11736-11742.
41. X. Hou, Y. J. Liu, H. Dong, F. Yang, L. Li and L. Jiang, *Adv. Mater.*, 2010, **22**, 2440-2443.
42. H. Zhang, X. Hou, L. Zeng, F. Yang, L. Li, D. Yan, Y. Tian and L. Jiang, *J. Am. Chem. Soc.*, 2013, **135**, 16102-16110.
43. M. Ali, P. Ramirez, H. Q. Nguyen, S. Nasir, J. Cervera, S. Mafe and W. Ensinger, *ACS Nano*, 2012, **6**, 3631-3640.
44. P. Y. Apel, I. Blonskaya, A. Y. Didyk, S. Dmitriev, O. Orelovitch, D. Root, L. Samoilova and V. Vutsadakis, *Nucl. Instrum. Methods Phys. Res., Sect. B*, 2001, **179**, 55-62.
45. P. Y. Apel, I. Blonskaya, O. Orelovitch and S. Dmitriev, *Nucl. Instrum. Methods Phys. Res., Sect. B*, 2009, **267**, 1023-1027.
46. Y. Xie, X. Wang, J. Xue, K. Jin, L. Chen and Y. Wang, *Appl. Phys. Lett.*, 2008, **93**, 163116.
47. Z. P. Zeng, Y. Ai and S. Z. Qian, *Phys. Chem. Chem. Phys.*, 2014, **16**, 2465-2474.
48. X. Hou, H. Dong, D. Zhu and L. Jiang, *Small*, 2010, **6**, 361-365.
49. P. Y. Apel, Y. E. Korchev, Z. Siwy, R. Spohr and M. Yoshida, *Nucl. Instrum. Methods Phys. Res., Sect. B*, 2001, **184**, 337-346.
50. K. Xiao, G. Xie, Z. Zhang, X. Y. Kong, Q. Liu, P. Li, L. Wen and L. Jiang, *Adv. Mater.*, 2016, DOI: 10.1002/adma.201505842.
51. Q. H. Nguyen, M. Ali, S. Nasir and W. Ensinger, *Nanotechnology*, 2015, **26**, 485502.
52. D. Mo, J. D. Liu, J. L. Duan, H. J. Yao, H. Latif, D. L. Cao, Y. H. Chen, S. X. Zhang, P. F. Zhai and J. Liu, *Nucl. Instrum. Methods Phys. Res., Sect. B*, 2014, **333**, 58-63.
53. J. M. Perry, K. Zhou, Z. D. Harms, S. C. Jacobson , ACS Nano, 2010, **4**, 3897-3903.

RSC Advances Accepted Manuscript

This journal is © The Royal Society of Chemistry 20xx

54. L. Gao, P. Li, Y. Zhang, K. Xiao, J. Ma, G. Xie, G. Hou, Z. Zhang, L Wen, L. Jiang. Small, 2015, **11**, 543-549.
55. Y. Shang, Y. Zhang, P. Li, J. Lai, X-Y. Kong, W. Liu, K. Xiao, G. Xie, Y. Tian, L. Wen. Chem. Commun., 2015, **51**, 5979-5982.
56. P. Y. Apel, I. V. Blonskaya, O. L. Orelovitch, B. A. Sartowska and R. Spohr, *Nanotechnology*, 2012, **23**, 225503.
57. I. Vlassiouk, S. Smirnov and Z. Siwy, *Acs Nano*, 2008, **2**, 1589-1602.
58. R. Karnik, C. Duan, K. Castelino, H. Daiguji and A. Majumdar, *Nano Lett.*, 2007, **7**, 547-551.
59. Z. Siwy, I. Kosińska, A. Fuliński and C. Martin, *Phys. Rev. Lett.*, 2005, **94**, 048102.
60. I. Kosińska and A. Fuliński, *Phys. Rev. E*, 2005, **72**, 011201.
62. D. Stein, M. Kruithof and C. Dekker, *Phys. Rev. Lett.*, 2004, **93**, 035901.
63. E. R. Cruz-Chu, T. Ritz, Z. S. Siwy and K. Schulten, *Faraday. Discuss.*, 2009, **143**, 47-62.
64. J. Cervera, B. Schiedt and P. Ramirez, *Europhys. Lett.*, 2005, **71**, 35.

RSC Advances Accepted Manuscript

TOC

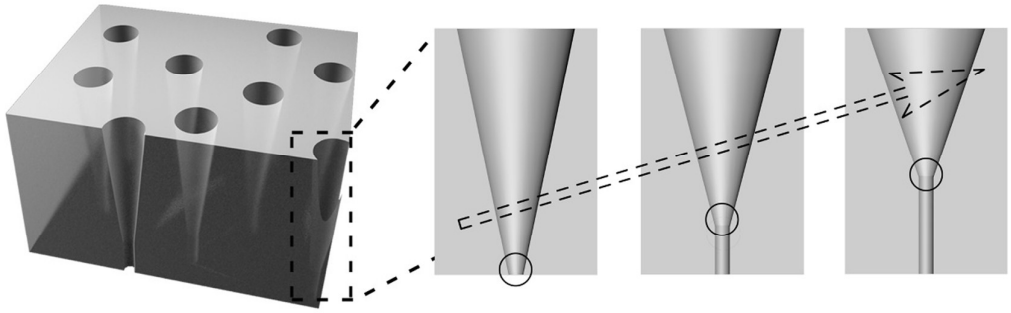

TOC: We demonstrate the funnel-shaped nanochannels with a gradual structural transformation and controlled ionic transportation properties.

RSC Advances Accepted Manuscript